Analysis and Control of Transient Torque Response in Engines with Internal Exhaust Gas Recirculation

Anna G. Stefanopoulou, *Member, IEEE,* and Ilya Kolmanovsky, *Member, IEEE*

***Abstract*— In this paper we analyze the nonlinear dynamic behavior of an internal exhaust gas recirculation system based on a mean-value model of an experimental automotive engine equipped with a camshaft phaser. We develop a control scheme that adjusts camshaft timing to reduce feedgas emissions while maintaining transient engine torque response similar to that of a conventional engine with zero exhaust gas recirculation. The control scheme consists of a feedforward map that specifies desired camshaft timing as a function of throttle position and engine speed in steady state, and a first-order lag that governs the transition of the camshaft timing to the desired value. The time constant of the first-order lag is adjusted based on engine speed and throttle position.**

***Index Terms*—Dynamic response, emissions, internal combustion engines, poles and zeros, pollution control, modeling, torque control.**

I. Introduction

THE exhaust gas recirculation (EGR) was introduced in the early 1970's to control the formation of oxides of nitrogen (NO_x) in internal combustion engines and thus reduce one of the main pollutants in automobile exhausts. The limits on acceptable NO_x emissions from passenger vehicles are stringently regulated by governments around the world. The recirculated inert exhaust gases dilute the inducted air-fuel charge and lower the combustion temperature which reduces NO_x feedgas emissions. Conventionally, exhaust gas recirculation is accomplished by controlling the exhaust gas that is supplied from the exhaust manifold to the intake manifold through a vacuum actuated valve. The EGR control algorithm is a simple proportional integral (PI) or proportional integral derivative (PID) loop that adjusts the valve position to the scheduled steady-state value. Exhaust gas recirculation alters the breathing process dynamics and consequently the torque response. Careful steady-state and transient control design is necessary to maintain good engine torque response. For this reason, EGR is typically turned off or is considerably delayed in transient engine operations, engine warm-up, and idling.

The advances in real-time computing and hardware are making possible the application of fully controlled valve events. Optimized valve events can improve the gas exchange process and enable control of internal EGR. Variable camshaft timing is an innovative and simple mechanical design approach for controlling EGR. By retarding the camshaft timing as shown in Fig. 1, combustion products which would otherwise be expelled during the exhaust stroke are retained in the cylinder during the subsequent intake stroke. This is a method of phasing the camshaft to control residual dilution and achieve the same results as with the conventional external EGR system.

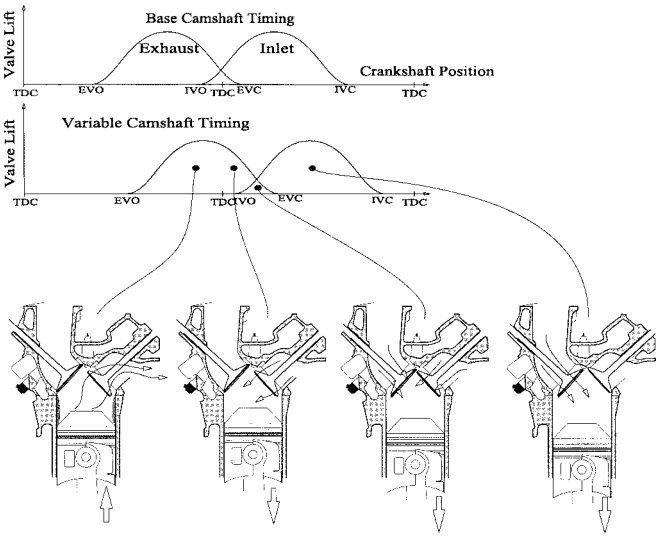

Fig. 1. Schematic picture of a cylinder with variable valve motion. In this scheme, the valve overlap occurs later during the intake event. This causes the induction of the last part of the exhaust gases into the cylinder. The resulting dilution lowers the combustion temperature and suppresses feedgas NO_x emissions.

Achieving exhaust gas recirculation through the exhaust manifold during the intake stroke is a better way of controlling the residual mass fraction during transients because 1) we eliminate the long transport delay associated to the exhaust-to-intake manifold path and 2) we bypass the slow dynamics associated with the intake manifold filling dynamics. Fast transient control of the internal exhaust gas recirculation (IEGR) is only limited by the camshaft phasor dynamics and computational delays. At a first glance, this suggests a possibility of better transient control of feedgas emissions than can be achieved with the conventional external exhaust gas recirculation (EEGR). Analysis of the IEGR system in throttled engines shows, however, that the IEGR system interacts with the slow intake manifold filling dynamics and can cause, in fact, unacceptable engine performance [6]. To improve

Manuscript received September 3, 1997. Recommended by Associate Editor, G. J. Rogers. This work was supported in part by the National Science Foundation under Contracts ECS-97-33293; matching funds to these Grants were provided by Ford Motor Co.

A. G. Stefanopoulou is with the Mechanical and Environmental Engineering Department, University of California, Santa Barbara CA 93106 USA.

I. Kolmanovsky is with the Ford Motor Company, Scientific Research Laboratory, Dearborn, MI 48121-2053 USA.

Publisher Item Identifier S 1063-6536(99)06450-7.

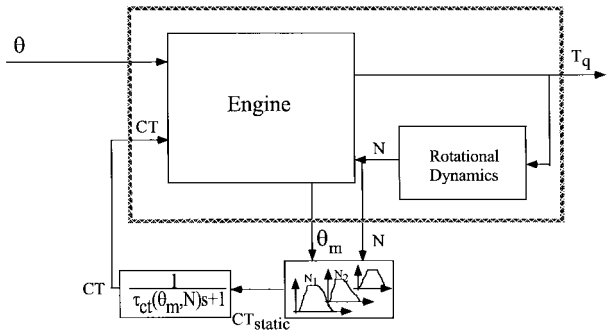

Fig. 2. Control structure.

the engine performance and reject the undesirable effects in torque response additional actuators can be employed, such as electronic throttle in [2] and air-bypass valve in [3]. However, the authority of the air-bypass valve may not be sufficient to compensate for torque disturbances due to camshaft motion and electronic throttle is at present not available on most production engines for cost reasons.

In this paper we analyze the nonlinear dynamic behavior of the IEGR system based on the mean-value model of an experimental engine equipped with a camshaft phaser [5]. We develop a dynamic camshaft timing schedule that regulates IEGR while maintaining transient engine torque response similar to an engine with zero EGR. The torque response of an engine with zero EGR provides the benchmark for the engine performance that we wish to achieve because any level of EGR can cause severe torque hesitation if not well calibrated.

Modularity of the IEGR control function is another very important requirement for the control design. Modular IEGR control function will allow its rapid implementation in existing real-time engine controllers. For this reason, the IEGR controller architecture that we develop can be seamlessly added or removed from the powertrain controller depending on the platform needs. The torque response requirement is achieved with no need for additional actuator regulating the flow into the intake manifold. Fig. 2 shows the developed IEGR control architecture. We dynamically schedule the camshaft timing (CT) that regulates IEGR based on the measured throttle angle (θ_m) and engine speed (N). Briefly stated here, the dynamic schedule consists of 1) the steady-state camshaft timing values (CT) for all throttle and engine speeds and 2) the time constant (τ_{ct}) of the first-order differential equation that defines the transient behavior of IEGR from one steady-state point to the next. The time constant is selected as a function of engine speed and throttle position as required to meet the torque response requirements.

II. Internal EGR System

The mean-value model of an experimental engine with variable camshaft timing shows that significant NO_x reduction can be achieved by allowing the exhaust valve to remain open for a longer period of time during the intake stroke. This is achieved by increasing the fraction of exhaust gases into the cylinder. The experimental data in Fig. 3 demonstrate the correlation between NO_x formation and percentage of external

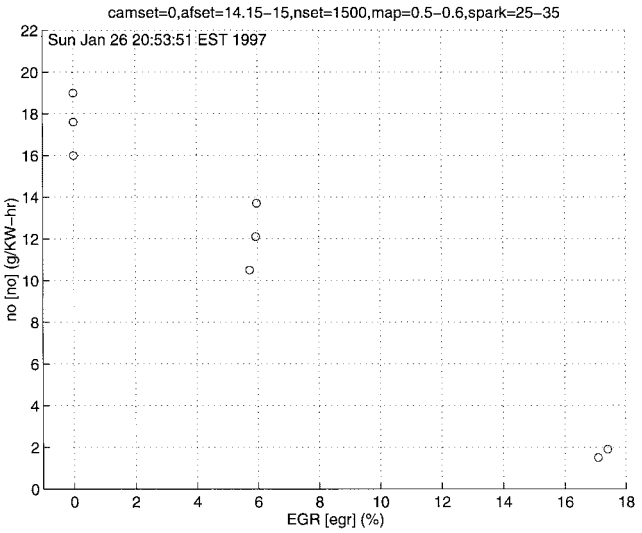

Fig. 3. Effects of external exhaust gas recirculation (EGR) on feedgas NO_x.

EGR flow. As the heading in Fig. 3 indicates, the data were collected using conventional camshaft timing $(camset = 0)$, stoichiometric air-to-fuel ratio $(afrset = 14.1515.00)$, engine speed at 1500 r/min $(nset = 1500)$ intake manifold pressure 0.5–0.6 bar $(map = 0.50.6)$, and spark timing 25–35° $(spark = 2535)$. Note here that to demonstrate the correlation between EGR flow and NO_x formation, it is important to fix all other engine variables. Similarly, the experimental data in Fig. 4 show the effects of camshaft timing (CT) on the feedgas NO_x generation in an IEGR engine. Note again that the experimental data correspond to the same engine conditions as in Fig. 3 and zero external EGR flow $(egrset = 0)$. Retarding camshaft timing increases the IEGR[1] and that results in reduction in feedgas NO_x. From Fig. 4 it is obvious that to reduce feedgas NO_x we have to ensure engine operation with maximum CT.

At the same time CT lowers the volumetric efficiency of the engine as shown in Fig. 5 allowing less mass of fresh air into the cylinders. The mean mass flow rate of fresh air into the cylinders $(\dot{m}_{\text{cyl}})$ is a function of volumetric efficiency (η), the intake manifold air density (ρ_m), the engine displacement (V_d), and engine speed (N)

$$\dot{m}_{\text{cyl}} = \eta \rho_m V_d \frac{N}{120}. \tag{1}$$

The volumetric efficiency measures the effectiveness of an engine's induction process and is defined as the ratio of mass of air inducted in the cylinders over one engine cycle to the mass of air contained in engine displacement volume at the intake manifold density [1]. Using the continuity equation for air flow into $(\dot{m}_\theta)$ and out $(\dot{m}_{\text{cyl}})$ of the intake manifold, and

[1] The simple relationship "increasing camshaft timing (CT) increases IEGR" is used throughout this paper. A mathematical equation describing the relationship between CT and IEGR is not available because it is difficult to measure EGR mass inside the cylinder.

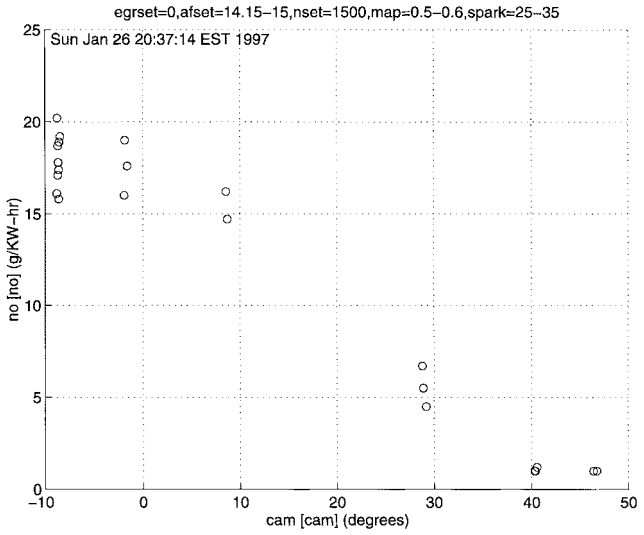

Fig. 4. Effects of camshaft timing (CT) on feedgas NO_x.

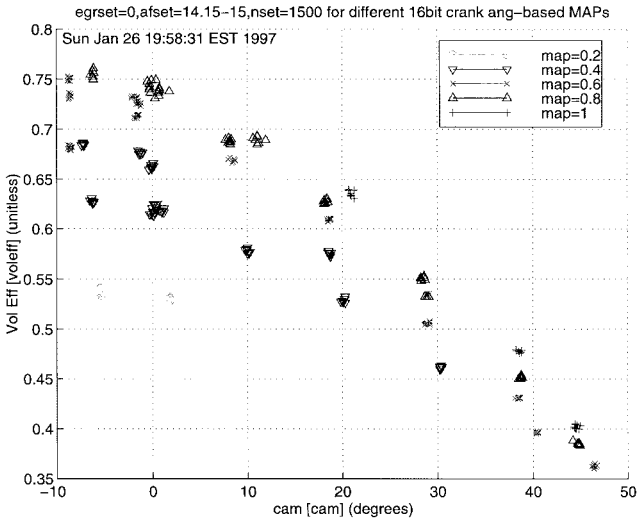

Fig. 5. Volumetric efficiency as a function of camshaft timing for different manifold pressures at 1500 r/min.

the ideal gas law assuming constant air temperature (T_m)[2] we describe the intake manifold pressure (P_m)

$$\frac{d}{dt}P_m = k_m(\dot{m}_\theta - \dot{m}_{\text{cyl}}). \tag{2}$$

The air flow into the intake manifold $(\dot{m}_\theta)$ can be computed by the discharge coefficient at the throttle plate $(A(\theta))$ and the pressure difference across the throttle plate (P_{ambient}/P_m). Using the regression equations in [5] we can describe the breathing process of the IEGR system

$$\begin{aligned} \dot{m}_\theta &= F_1(P_m, \theta) \\ \frac{d}{dt}P_m &= k_m(\dot{m}_\theta - \dot{m}_{\text{cyl}}) \\ \dot{m}_{\text{cyl}} &= F_2(CAM, P_m, N). \end{aligned} \tag{3}$$

[2]In contrast to the conventional EGR systems, the internal exhaust gas recirculation system described in this paper maintains constant intake manifold temperature for different level of EGR recirculation. This happens because, the exhaust gas recirculation is achieved through the exhaust manifold and not the intake manifold.

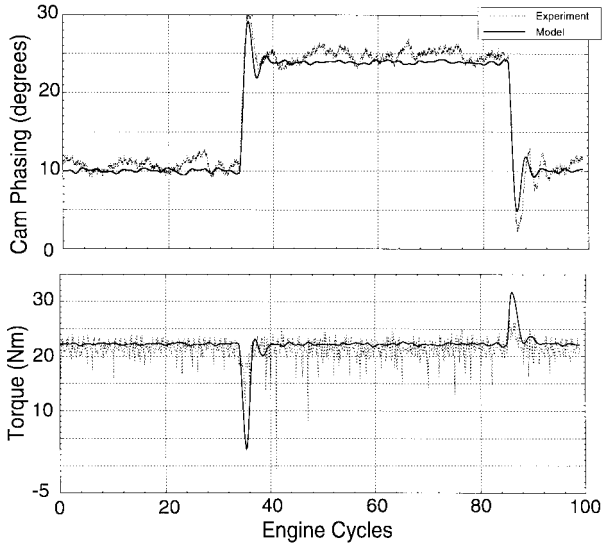

Fig. 6. Effect of camshaft phasing on torque: simulation and experimental results.

In-cylinder torque generation can be simply computed using an empirical function of the mass air flow into the cylinder $(\dot{m}_{\text{cyl}})$, the air-to-fuel (A/F) ratio, the spark timing (σ), and the engine speed (N)

$$T_q = F_3(\dot{m}_{\text{cyl}}, \sigma, N, A/F). \tag{4}$$

Our goal is to schedule IEGR without the detrimental consequences to engine torque response shown in Fig. 6. For simplicity, we will assume precise A/F ratio and spark control. We will also analyze the effects of IEGR on engine torque response assuming constant engine speed and schedule IEGR as a function of engine speed. With these two assumptions, the engine torque response is determined by the mass air flow into the cylinder. We use the time-based mean-value engine model described in detail in [5] and summarized here with (3) and (4) instead of the crank-based engine dynamics because the camshaft timing actuator dynamics and the desired torque response that satisfies driveabilty are treated easier in the time domain. The prediction ability of the model described by (3) and (4) is demonstrated in Fig. 6, where experimental and simulation data are plotted.

III. Static Schedule

Exhaust gas recirculation decreases the engine torque response. Fig. 7 shows the normalized torque response for zero IEGR (dashed line) and for the maximum IEGR (dashed-dot line) that the engine can achieve. The normalized torque is given as a function of throttle angle for constant engine speed. To minimize feedgas emissions we need to operate at maximum IEGR. To ensure maximum torque at wide open throttle (WOT) we need to reduce IEGR back to zero. The solid line in Fig. 7 shows such a smooth transition from maximum IEGR for part throttle to zero IEGR for WOT. For very small throttle angles (small air flow into the cylinders) IEGR deteriorates the combustion stability because of the high level of dilution. IEGR, therefore, is scheduled at zero for

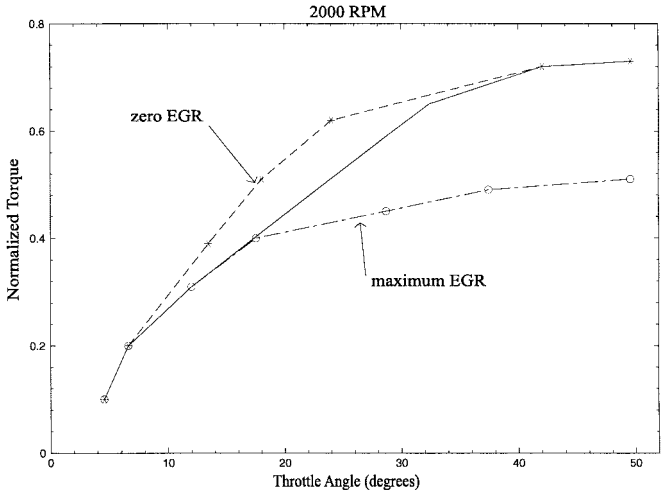

Fig. 7. Comparison between static normalized torque response for zero IEGR, maximum IEGR, and a realizable IEGR scheme.

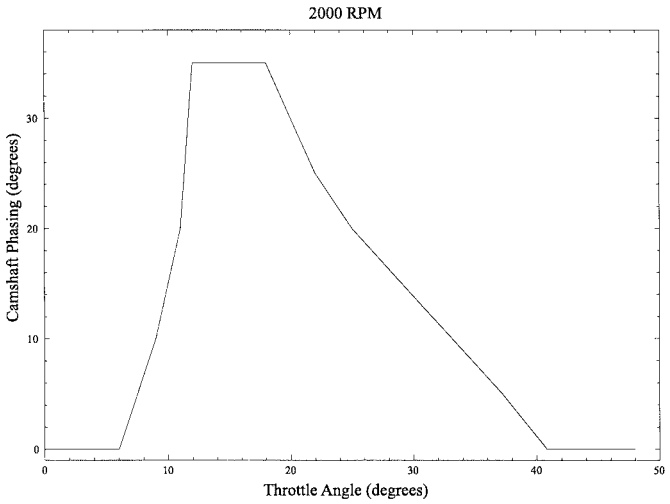

Fig. 8. The static camshaft scheduling scheme at 2000 r/min.

small throttle angles to maintain combustion stability. Using the above guidelines we derive the static camshaft timing (CT_{static}) as follows: 1) near idle it is scheduled for idle stability which requires cam phasing equal to zero; 2) at mid-throttle it is scheduled for emissions which favors fully retarded cam phasing; and 3) at WOT it is scheduled for maximum torque which requires camshaft timing to be advanced back to 0°. The developed camshaft scheduling scheme, shown in Fig. 8, ensures reduction of feedgas emissions under the constraint of smooth steady-state torque response for engine speed equal to 2000 r/min.

This steady-state map can be derived based on different static optimization schemes depending on static engine performance tradeoffs that satisfy design requirements. We chose pedal position and engine speed as inputs to this map to allow modular implementation of the control strategy. Throttle position is a natural independent variable for the camshaft control scheme. Engine speed, although not independent, is a slowly varying parameter, which implies that it can be safely used as the second scheduling parameter. The problem that remains unsolved is the transition characteristics from one static IEGR point to the next set point as the steady-state map requires. To minimize feedgas emissions we want to change camshaft timing (CT) to the optimum position (CT_{static}) as fast as possible or as fast as the actuator bandwidth allows.

IV. Analysis of Transient Torque Response

In this section we analyze the effects of the speed of response of the CT on the transient torque response of the engine. We assume that the IEGR dynamics are first-order, characterized by

$$\frac{d}{dt}CT = \frac{1}{\tau_{ct}}(-CT(t) + CT_{\text{static}}(\theta(t), N(t))) \qquad (5)$$

where the time-constant τ_{ct} determines the speed with which CT is changed. As in the previous section, we assume a tight A/F ratio and spark control loop which implies that the torque response is determined by the air flow response. Fig. 9 shows the torque response of the IEGR engine to an instantaneous throttle change for the two constant engine speed values of 750 and 2000 r/min. When the throttle angle changes instantaneously at $t = 0$ to a new value θ_m, the CT changes to a new value, $CT_{\text{static}}(\theta_m, N)$, according to

$$CT(t) = \exp(-t/\tau_{ct})CT(0) + (1 - \exp(-t/\tau_{ct})) \cdot CT_{\text{static}}(\theta, N), \qquad t \geq 0. \qquad (6)$$

The three different torque profiles in Fig. 9 result for the three different values of τ_{ct}. If the CT changes fast (τ_{ct} is small) the torque response may exhibit an undershoot. This happens because of the tendency of the air flow to decrease with the increase in CT. If the CT changes slowly (τ_{ct} is large) the torque may overshoot. This happens because the air flow first increases quickly due to the intake pressure dynamics caused by a larger throttle angle; then the air flow decreases due to the CT slowly approaching the desired, larger than the initial, value. From the driver's perspective both, the undershoot and the overshoot, are undesirable.

The above intuitive arguments showing that the speed of CT adjustment affects the engine torque response can be supported analytically. In Section IV-A we analyze the air flow response to a throttle step and we confirm analytically the intuitive observations that we made above. The response to a throttle step from an equilibrium can be also viewed as a response to the initial condition corresponding to this equilibrium. However, if frequent aggressive throttle steps occur the system may not have enough time to reach a sufficiently small neighborhood of the equilibrium before the next throttle step occurs. In this situation, the analysis of response to general initial conditions may be more appropriate than the analysis of the step response. We present this initial condition response analysis in Section IV-B assuming that engine speed and throttle are fixed. The linear time invariant system that we are using in the following sections is derived by linearizing (3):

$$\Delta\dot{m}_{\theta}(t) = k_{\theta 1}\Delta\theta(t) - k_{\theta 2}\Delta P_m(t)$$
$$\Delta\dot{m}_{\text{cyl}}(t) = -k_{p1}\Delta CT(t) + k_{p2}\Delta P_m(t)$$

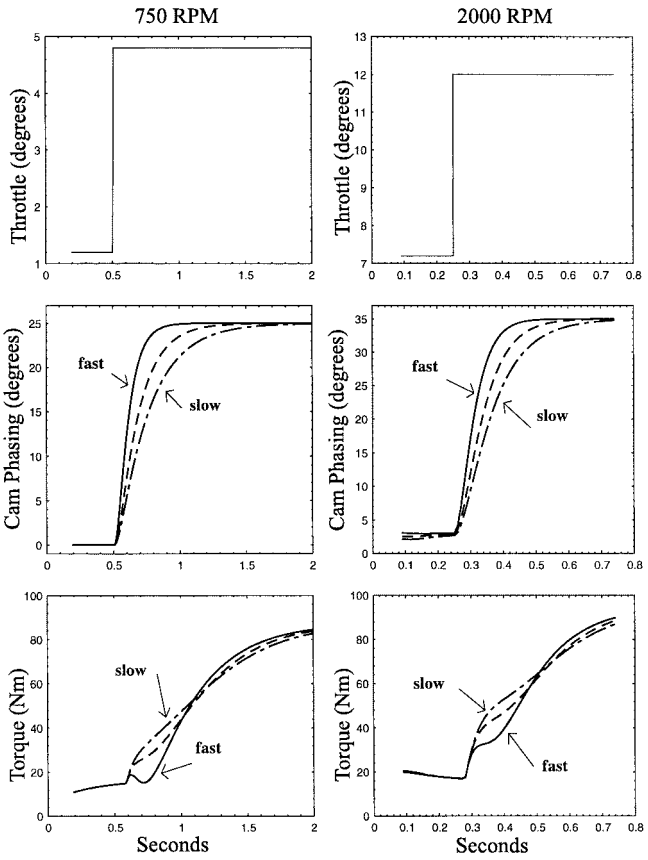

Fig. 9. Torque response (at 750 and 2000 r/min) using different camshaft dynamic characteristics.

$$\frac{d}{dt}\Delta P_m(t) = k_m(\Delta \dot{m}_\theta(t) - \Delta \dot{m}_{\text{cyl}}(t)) \tag{7}$$

where $k_{\theta i} \geq 0$, $k_{pi} \geq 0$ for $i = 1, 2$ and $k_m > 0$. Linearization of the dynamic camshaft timing scheme results in

$$\frac{d}{dt}\Delta CT(t) = \frac{1}{\tau_{ct}}(-\Delta CT(t) + k_o \Delta\theta(t)) \tag{8}$$

where $k_o = (\partial(CT_{\text{static}})/\partial\theta)$ depends on throttle angle and engine speed. The gain k_o in contrast to all other gains (k_i's) that are nonegative may take both positive and negative values for different operating points as described in Section III and shown in Fig. 8.

A. Analysis of Response to Throttle Steps

The transfer function between camshaft timing, throttle position, and mass air flow into the cylinders is given by

$$\Delta \dot{m}_{\text{cyl}}(s) = \frac{k_m k_{\theta 1} k_{p2}}{s + k_m(k_{\theta 2} + k_{p2})}\Delta\theta(s) - \frac{k_m k_{p1} k_{\theta 2} + k_{p1} s}{s + k_m(k_{\theta 2} + k_{p2})}\Delta CT(s). \tag{9}$$

Substitution of the linear camshaft scheduling scheme

$$\Delta CT(s) = \frac{k_o}{\tau_{ct} s + 1}\Delta\theta(s) \tag{10}$$

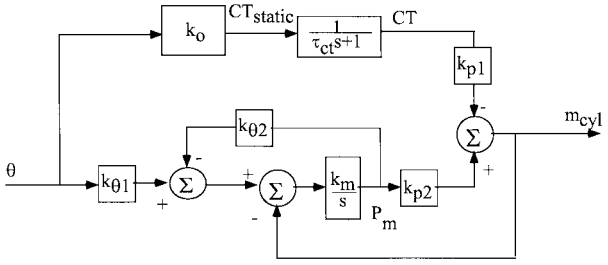

Fig. 10. Block diagram of the linear IEGR system.

to (10) results in the transfer function from throttle angle to cylinder air flow for the closed-loop IEGR system

$$\frac{\Delta \dot{m}_{\text{cyl}}(s)}{\Delta\theta(s)} = k_m k_{p2} \cdot \frac{\left(k_{\theta 1}\tau_{ct} - k_o \frac{k_{p1}}{k_m k_{p2}}\right)s + \left(k_{\theta 1} - k_o k_{\theta 2}\frac{k_{p1}}{k_{p2}}\right)}{(\tau_{ct} s + 1)[s + k_m(k_{\theta 2} + k_{p2})]}. \tag{11}$$

The block diagram of the linear IEGR system is shown in Fig. 10. For simplicity we rewrite (11) in terms of its dc gain (k_{dc}^{st}), poles and zero

$$\Delta \dot{m}_{\text{cyl}} = T_{\text{IEGR}}^{st}(s)\Delta\theta$$
$$T_{\text{IEGR}}^{st}(s, \tau_{ct}) = k_{dc}^{st}\frac{\frac{s}{z} + 1}{\left(\frac{s}{p_{ct}} + 1\right)\left(\frac{s}{p_m} + 1\right)} \tag{12}$$

where

$$k_{dc}^{st} = \frac{k_{p2}k_{\theta 1} - k_{p1}k_{\theta 2}k_o}{k_{\theta 2} + k_{p2}}$$
$$z = \frac{k_{\theta 1} - k_o k_{\theta 2}\frac{k_{p1}}{k_{p2}}}{k_{\theta 1}\tau_{ct} - k_o\frac{k_{p1}}{k_m k_{p2}}}$$
$$p_{ct} = \frac{1}{\tau_{ct}}, \quad \text{and} \quad p_m = k_m(k_{\theta 2} + k_{p2}).$$

Proposition: The necessary and sufficient condition for the step response of (12) to be monotonic is

$$z \geq \min\{p_m, p_{ct}\}. \tag{13}$$

This result follows from the general conditions for the monotonic step response, see [4]. It can also be derived directly by writing out the step response shown in (12) in the time domain.

We use the notation $p_m(\theta, N)$, $z(\theta, N, \tau_{ct})$, $p_{ct}(\tau_{ct})$ to indicate the dependence of the poles and zeros of the IEGR engine transfer function on the operating point and the dynamic schedule. For small values of τ_{ct}, we have a nonminimum phase zero ($z < 0$) if $k_o > 0$. This follows because $1 - k_o(k_{\theta 2}/k_{\theta 1})(k_{p1}/k_{p2})$ is positive since $1 - k_o(k_{\theta 2}/k_{\theta 1})(k_{p1}/k_{p2}) = (k_{dc}^{st}/(k_{p2}k_{\theta 1}))$, and the static schedule ensures $k_{dc}^{st} > 0$ for all engine conditions. As τ_{ct} increases, the zero z converges to the origin at a rate equal to $1/(1 - k_o(k_{\theta 2}/k_{\theta 1})(k_{p1}/k_{p2})) < 1$. The pole p_{ct} converges

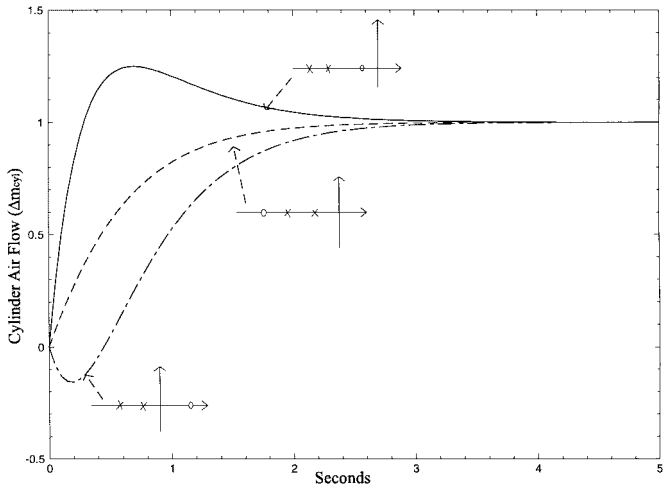

Fig. 11. Qualitative cylinder air flow behavior of the IEGR system for different pole zero location.

to the origin slower, at a rate equal to one. Hence, for large values of τ_{ct} the zero z is to the right of the pole p_{ct}, and torque exhibits an overshoot. Thus the admissible range for τ_{ct} that guarantees monotonic step responses is a bounded interval that can be computed from (12) and (13).

To summarize and relate the above analysis to the physical system consider the following scenarios. If an aggressive IEGR dynamic schedule has to be implemented to reduce feedgas emissions, the small time constant τ_{ct} might cause torque response to undershoot during step throttle changes (dot-dashed line in Fig. 11). If hardware limitations impose bandwidth constraints in the dynamic IEGR response, then the large time constant τ_{ct} might cause torque response to overshoot (zero to the right of the largest pole p_{ct}, solid line in Fig. 11), or to respond slowly to the torque demand due to the dominant slow pole p_{ct} (dashed line in Fig. 11). These conclusions hold in the region where the static schedule calls for cam phasing increase in response to throttle angle increase $(k_o > 0)$.

In the region of high manifold pressure (normal flow, $k_{\theta 2} > 0$) the static schedule requires $k_o < 0$, i.e., we start decreasing the dilution to achieve the maximum engine torque (see Section III). In this case it can be verified that admissible values for τ_{ct} must be either sufficiently large or sufficiently small (see Appendix B).

B. Analysis of Initial Condition Response

Let $x_1 = \Delta P_m$, $x_2 = \Delta CT$, $x = (x_1 \vdots x_2)^T$, $y = \Delta \dot{m}_{\text{cyl}}$. The system shown in (7) and (8) with $\Delta\theta = 0$ can be written as

$$\begin{aligned} \dot{x} &= Ax \\ y &= Cx \end{aligned} \tag{14}$$

where

$$\begin{aligned} A &= \begin{pmatrix} a_{11} & a_{12} \\ 0 & a_{22} \end{pmatrix}, \quad C = (c_1 \vdots c_2) \\ a_{11} &= -k_m k_{\theta 2} - k_m k_{p2}, \quad a_{12} = k_{p1} k_m \\ a_{22} &= -\frac{1}{\tau_{ct}}, \quad c_1 = k_{p2}, \quad c_2 = -k_{p1}. \end{aligned} \tag{15}$$

We are interested in the range of values for τ_{ct}, x_{01} and x_{02} for which the air flow response of the system in (14) due to the initial condition is monotonic for $0 < t < \infty$. To utilize simple necessary and sufficient conditions for the monotonic response of the system in (14) we derive a system with identical unit step response. It can be verified that the response of the system in (14) to an initial condition $x(0) = x_0 = (x_{01} \vdots x_{02})^T$ coincides with the step response of the system

$$\begin{aligned} \dot{\zeta} &= A\zeta + (Ax_0)u \\ y &= C\zeta + (Cx_0)u \end{aligned} \tag{16}$$

with a zero initial condition $\zeta(0) = 0$ for $0 < t < \infty$. The transfer function of the system in (16) is

$$T^{ic}_{\text{IEGR}}(s, \tau_{ct}) = \frac{h_1 s + h_2}{(s - a_{11})(s - a_{22})} + c_1 x_{01} + c_2 x_{02} \tag{17}$$

where

$$\begin{aligned} h_1 &= c_1 a_{11} x_{01} + c_1 a_{12} x_{02} + c_2 a_{22} x_{02} \\ h_2 &= -c_1 a_{22} a_{11} x_{01} - c_2 a_{11} a_{22} x_{02}. \end{aligned}$$

As in the previous section, we define

$$p_{ct} = -a_{22}, \quad p_m = -a_{11}$$

and obtain

$$\begin{aligned} T^{ic}_{\text{IEGR}}(s, \tau_{ct}) = \frac{h_2}{p_m p_{ct}} \; & \frac{\dfrac{h_1}{h_2} s + 1}{\left(\dfrac{s}{p_m} + 1\right)\left(\dfrac{s}{p_{ct}} + 1\right)} \\ & + c_1 x_{01} + c_2 x_{02}. \end{aligned} \tag{18}$$

The response of the system in (16) to an initial condition $x(0) = x_0 = (x_{01} \vdots x_{02})^T$ is monotonic if and only if the step response of the system without D-term

$$\begin{aligned} \dot{\zeta} &= A\zeta + (Ax_0)u \\ y &= C\zeta \end{aligned}$$

$$\overline{T}^{ic}_{\text{IEGR}}(s, \tau_{ct}) = \frac{h_2}{p_m p_{ct}} \; \frac{\dfrac{h_1}{h_2} s + 1}{\left(\dfrac{s}{p_m} + 1\right)\left(\dfrac{s}{p_{ct}} + 1\right)} \tag{19}$$

with a zero initial condition, $\zeta(0) = 0$, is monotonic for $0 < t < \infty$. Using the pole-zero condition obtained in the previous section, we require

$$\frac{h_2}{h_1} \geq \min\{p_m, p_{ct}\}. \tag{20}$$

Note that h_1 and h_2 depend linearly on x_{01} and x_{02}. Hence, the set of x_{01}, x_{02} for which the response of the system in (14) is monotonic, $X_0(\tau_{ct}, \theta, N)$, is a union of two conically shaped regions

$$\begin{aligned} X_0(\tau_{ct}, \theta, N) = \{x_0 &: K_1 x_0 \geq 0, K_2(\tau_{ct}) x_0 \geq 0 \quad \text{or} \\ & K_1 x_0 \leq 0, K_2(\tau_{ct}) x_0 \leq 0\} \end{aligned} \tag{21}$$

where

$$K_1 = (-c_1 p_m \,|\, -c_2 p_m)$$

$$K_2(\tau_{ct}) = \min\{p_m, (1/\tau_{ct})\}(c_1 p_m \,|\, -c_1 a_{12}) + (1/\tau_{ct})(K_1 + \min\{p_m, (1/\tau_{ct})\}(0 \,|\, c_2)).$$

The dependence of the set X_0 on the operating point is made clear by including θ and N in the list of arguments. The sets $X_0(\tau_{ct}, \theta, N)$ are positively invariant. That is, any trajectory of the system in (14) originating in $X_0(\tau_{ct}, \theta, N)$ remains in $X_0(\tau_{ct}, \theta, N)$.

It turns out that there is a value of τ_{ct}, τ_{ct}^*, for which all the initial conditions result in monotonic responses (see derivation in Appendix A)

$$\tau_{ct}^* = \frac{1}{k_m k_{\theta 2}}, \quad X_0(\tau_{ct}^*, \theta, N) = \boldsymbol{R}^2. \tag{22}$$

Note that the value of τ_{ct}^* is infinite for the operating points where the flow through the throttle is choking and is independent of P_m. For these operating points, $k_{\theta 2} = 0$ as follows from (7).

As an example, we compute the sets $X_0(\tau_{ct}, 15, 1300)$ for various values of τ_{ct}. For $\theta = 15, N = 1300$, $a_{11} = -p_m = -18.4$, $a_{12} = 0.06$, $c_1 = 31.2$, and $c_2 = -0.55$, we calculate

$$K_1 = (-573.2 \,|\, 10.1), \quad \text{and}$$

$$K_2(\tau_{ct}) = \min\left\{18.4, \frac{1}{\tau_{ct}}\right\}(573.2 \,|\, -1.88) + \frac{1}{\tau_{ct}}\left(K_1 + \min\left\{18.4, \frac{1}{\tau_{ct}}\right\}(0 \,|\, -0.55)\right).$$

For $\tau_{ct} \leq (1/p_m) = 0.054$, the set has a general appearance shown in Fig. 12. We used a specific value, $\tau_{ct} = 0.046$, to generate it. The cone region marked by "+" corresponds to initial conditions that result in monotonically increasing air flow while the one marked by "−" corresponds to initial conditions that result in monotonically decreasing air flow. As τ_{ct} increases and approaches the value of $(1/p_m) = 0.054$, the line $K_2 x_0 = 0$ becomes more and more horizontal and the set shrinks. We calculate, $\tau_{ct}^* = 0.067$. For $\tau_{ct} > 0.054$, the first element of $K_2(\tau_{ct})$ is zero and the line $K_2 x_0 = 0$ is horizontal. For $0.067 > \tau_{ct} > 0.054$ the set does not change although τ_{ct} changes, see Fig. 13. As τ_{ct} crosses the value of 0.067 the set flips over due to the second element of K_2 changing sign, see Fig. 14. For $\tau_{ct} > 0.067$ the set does not change when τ_{ct} changes. For the "flip over" value of 0.067, $K_2 = 0$ and all the initial conditions result in monotonic air flow responses, consistent with (22).

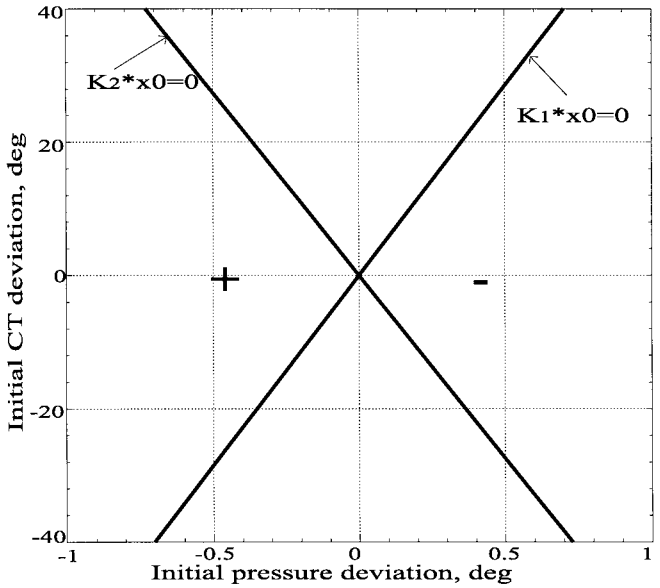

Fig. 12. The set $X_0(0.046\,15, 1300)$ is a union of two cone regions marked by "+" and "−."

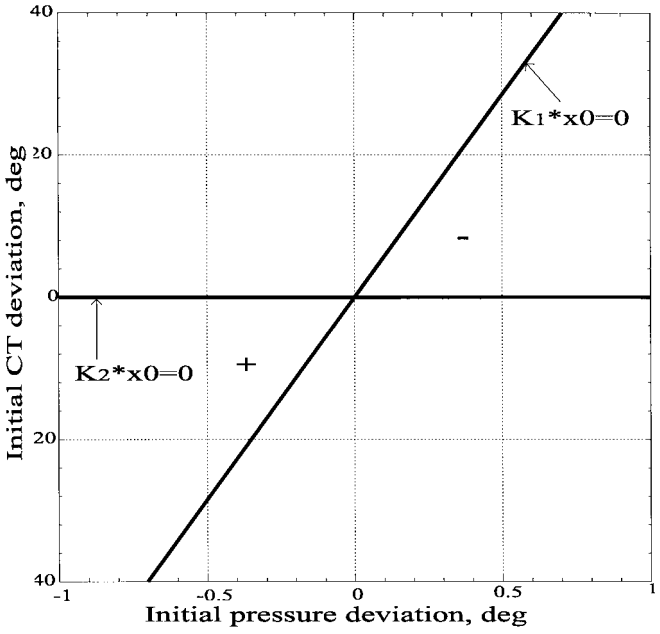

Fig. 13. The set $X_0(\tau_{ct}, 15, 1300)$ for $0.067 > \tau_{ct} > 0.054$ is a union of two cone regions marked by "+" and "−."

V. Target Transient Torque Response

Using appropriate values of the time constant of the first-order lag (τ_{ct}) we seek to minimize the differences between the cylinder air flow transients of an IEGR engine and an engine with zero EGR (ZEGR engine). The target dynamic response can be specified either by the transfer function from throttle angle to cylinder air flow for an engine with zero EGR or by the initial condition response of an engine with zero EGR. We consider these specifications in more detail in the remainder of this section.

The transfer function of the ZEGR engine with throttle input can be found by linearization of (3), after setting IEGR and hence camshaft timing equal to zero $(CT = 0)$

$$\Delta \dot{m}_{\text{cyl}}(s) = \frac{k_m k_{\theta 1} k_{p2}}{s + k_m(k_{\theta 2} + k_{p2})} \Delta\theta(s). \tag{23}$$

Note here that (23) can be derived also from (11) by assigning k_{p1} equal to zero. We can compare the two dynamical

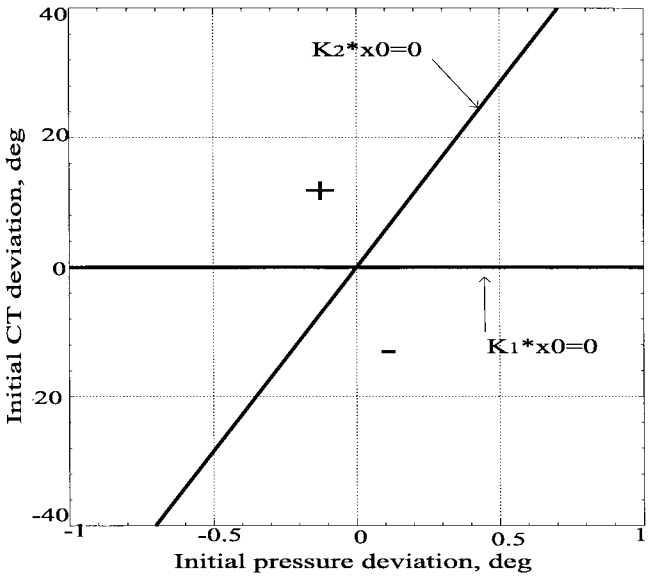

Fig. 14. The set $X_0(\tau_{ct}, 15, 1300)$ for $\tau_{ct} > 0.067$ is a union of two cone regions marked by "+" and "−."

systems after we rewrite the above transfer function with respect to its dc gain and pole location

$$\Delta \dot{m}_{\text{cyl}}(s) = T^{st}_{\text{ZEGR}}(s)\Delta\theta(s)$$
$$T^{st}_{\text{ZEGR}}(s) = \tilde{k}^{st}_{dc}\frac{1}{\frac{s}{p_m}+1}$$

where $\tilde{k}^{st}_{dc} = (k_{p2}k_{\theta 1}/k_{\theta 2} + k_{p2})$ and p_m as given in (13).

Table I summarizes the differences between the closed-loop transfer functions from throttle to cylinder air flow for the IEGR system and the ZEGR system
where

$$p_m = k_m(k_{\theta 2} + k_{p2}), \quad p_{ct} = \frac{1}{\tau_{ct}} \quad \text{and}$$
$$z = \frac{k_{\theta 1} - k_o k_{\theta 2}\dfrac{k_{p1}}{k_{p2}}}{k_{\theta 1}\tau_{ct} - k_o\dfrac{k_{p1}}{k_m k_{p2}}}.$$

As expected, the IEGR engine has considerably smaller dc gain than the ZEGR engine. Its dc gain depends on the static camshaft timing schedule $(k_o > 0)$ during subsonic flow $(k_{\theta 2} \neq 0)$. Although the target response is the ZEGR engine, we cannot match the DC gain of the ZEGR engine and there is no need to do so. The IEGR engine can meet the torque demand at higher throttle angle. Doing so will be beneficial to 1) fuel economy due to operation in higher manifold pressure which results in reduction in pumping losses [7] and 2) engine performance due to faster throttle to torque response at higher intake manifold pressure. Therefore, from the driver's perspective, the air flow response into the cylinders of the IEGR engine should match the air flow response into the cylinders of the ZEGR engine operating at the high manifold pressure equilibrium. For this reason the comparison is based on linearization of ZEGR engine model at the equilibrium pressure corresponding to the IEGR engine model [7]. We

TABLE I

	ZEGR Engine	IEGR Engine
Throttle Step Response	$T^{st}_{ZEGR}=\tilde{k}^{st}_{dc}\frac{1}{\frac{s}{p_m}+1}$	$T^{st}_{IEGR}=k^{st}_{dc}\frac{\frac{s}{z}+1}{(\frac{s}{p_m}+1)(\frac{s}{p_{ct}}+1)}$
DC Gain	$\tilde{k}^{st}_{dc}=\frac{k_{p2}k_{\theta 1}}{k_{\theta 2}+k_{p2}}$	$k^{st}_{dc}=\frac{k_{p2}k_{\theta 1}-k_{p1}k_{\theta 2}k_o}{k_{\theta 2}+k_{p2}}$

TABLE II

	ZEGR Engine	IEGR Engine
Equivalent Initial Condition Response	$T^{ic}_{ZEGR} =$ $\tilde{k}^{ic}_{dc}\left(\frac{1}{\frac{s}{p_m}+1}-1\right)$	$T^{ic}_{IEGR} =$ $k^{ic}_{dc}\left(\frac{\frac{h_1}{h_2}s+1}{(\frac{s}{p_m}+1)(\frac{s}{p_{ct}}+1)}-1\right)$
D-term	$\tilde{k}^{ic}_{dc}=-k_{p2}x_{01}$	$k^{ic}_{dc}=k_{p1}x_{02}-k_{p2}x_{01}$

thus assume that the values for p_m, $k_{\theta i}$, and k_{pi} for $i = 1, 2$ are the same when comparing the transfer functions of the two engine models.

Similarly, the initial condition response of the linearized IEGR model should be compared with the initial condition response of the ZEGR engine model, linearized at the equilibrium pressure of the IEGR engine model. If x_{01} is the initial pressure deviation, then, with throttle and engine speed fixed, the initial condition response of ZEGR engine for $0 < t < \infty$ coincides with the step response of a system with the transfer function

$$T^{ic}_{\text{ZEGR}}(s) = \frac{c_1 a_{11} x_{01}}{s - a_{11}} + c_1 x_{01} \tag{24}$$

and zero initial condition.

Table II summarizes the differences between the initial condition response of the ZEGR and the IEGR engine
where

$$p_m = k_m(k_{\theta 2} + k_{p2}), \quad p_{ct} = \frac{1}{\tau_{ct}}$$
$$\frac{h_2}{h_1} = \frac{(-k_{p2}x_{01} + k_{p1}x_{02})p_m p_{ct}}{-k_{p2}p_m x_{01} + k_{p1}(k_m k_{p2} + p_{ct})x_{02}},$$
$$x_{01} = P_m(0), \quad \text{and} \quad x_{02} = CT(0).$$

The differences in the dynamic characteristics of the two systems are due to the zero (z in step response, and h_2/h_1 in initial condition response) and the additional pole p_{ct} for the IEGR engine. The zero is the result of the interaction of the IEGR dynamics with the manifold filling dynamics. The pole is due to the the first-order lag of the dynamic schedule.

VI. Time Constant

In this section we find the time constant τ_{ct} that minimizes the combined effects of the zero and the additional pole p_{ct} in the IEGR air flow response. The basic idea is to select τ_{ct} for which the IEGR transient behavior is similar to the ZEGR engine behavior, a first-order lag with pole at p_m.

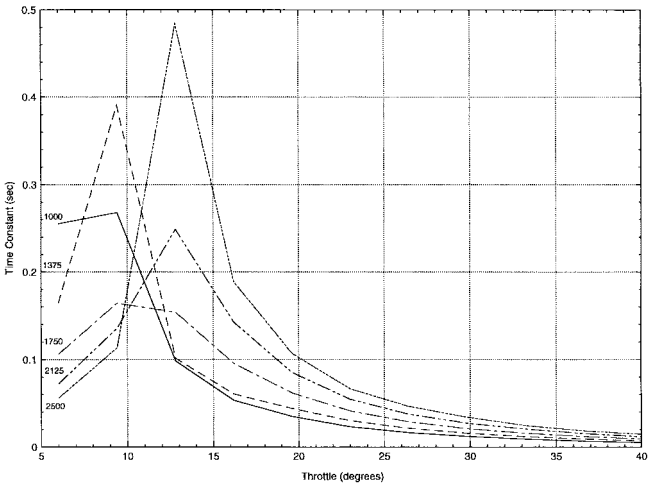

Fig. 15. The selected time constant τ_{ct} for different throttle angles and engine speeds.

The obvious choice of τ_{ct} that minimizes the difference of the two transfer functions

$$\frac{T^{st}_{\mathrm{IEGR}}(s)}{T^{st}_{\mathrm{IEGR}}(0)} \quad \text{and} \quad \frac{T^{st}_{\mathrm{ZEGR}}(s)}{T^{st}_{\mathrm{ZEGR}}(0)}$$

and satisfies the monotonicity constraint in Proposition 13 is $\tau^*_{ct} = (1/(k_m k_{\theta 2}))$. It leads to pole zero cancelation in T^{st}_{IEGR}, $p_{ct} = z$, thus matching the dynamic behavior (but not the dc gains) of the linearized IEGR and ZEGR engine models in response to throttle steps. Furthermore, it results in $(h_2/h_1) = p_{ct}$ and matches the dynamic behavior of the linearized IEGR and ZEGR engine models in response to initial conditions for $0 < t < \infty$. Note also that for $\tau_{ct} = \tau^*_{ct}$ all initial conditions result in monotonic zero input response of the IEGR engine, see (22).

In practice, it may not be possible to implement the value of τ^*_{ct} exactly thereby resulting in inexact pole zero cancelation and the "flip-over" effect described in Section IV-B. However, this should not be a matter of concern in practice because the response for the case of inexact implementation is sufficiently close to the one obtained for the exact value of τ^*_{ct}.

As we pointed out in Section IV-B, the choice $\tau_{ct} = \tau^*_{ct}$ is not feasible for the operating points for which the flow through the throttle is chocked because $k_{\theta 2} = 0$ and consequently τ^*_{ct} is infinite. Chocked flow through the throttle body occurs during small throttle angle for which k_o is nonegative (see Fig. 8). In this region we impose the monotonicity constraint, (13), which results in the following condition for τ_{ct}:

$$\frac{k_o k_{p1}}{k_{\theta 1} k_m k_{p2}} < \tau_{ct} < \frac{1}{k_m k_{p2}} + \frac{k_o k_{p1}}{k_{\theta 1} k_m k_{p2}}. \tag{25}$$

In Appendix B, we describe an algorithm that produces specific values for τ_{ct} that satisfy all of the above conditions. The values for τ_{ct} obtained by this algorithm for various operating points can be interpolated into a nonlinear static map (see Fig. 15), $\mathcal{T}$ so that

$$\tau_{ct}(t) = \mathcal{T}(\theta(t), N(t)). \tag{26}$$

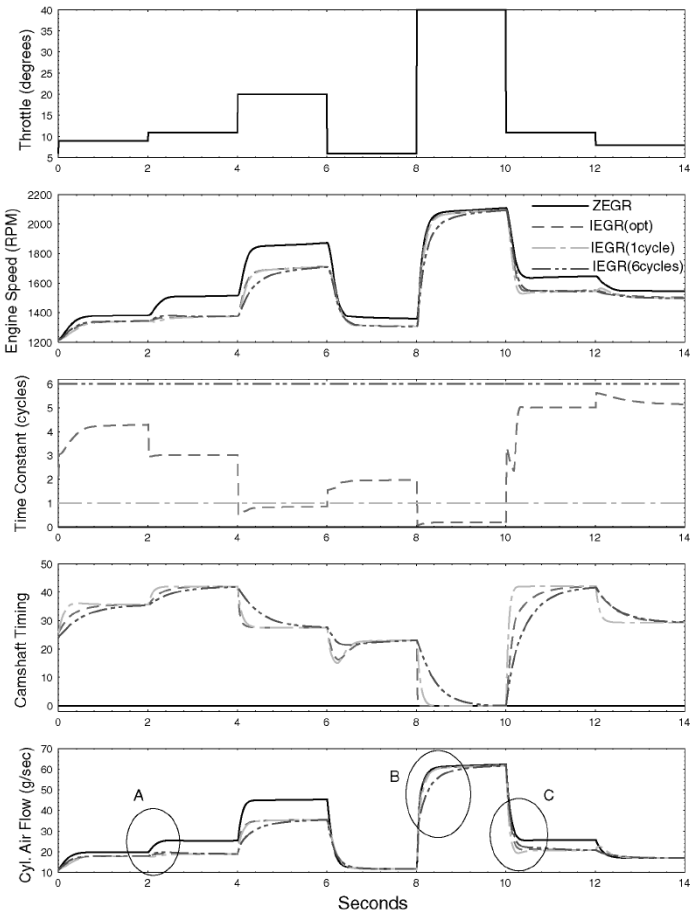

Fig. 16. Nonlinear simulation of 1) the zero EGR system (ZEGR); 2) the IEGR system with the optimized time constant (τ_{ct}); 3) the IEGR system for a small time constant [$IEGR$(one cycle)]; and 4) the IEGR system for a large time constant [$IEGR$(six cycles)].

Note that the specific procedure that we used to generate $\mathcal{T}$ is fairly involved computationally because it requires the linearization of the engine breathing dynamics. However, these computations are off-line and the on-line implementation of (26) is straightforward. A lookup table and linear interpolation are used to interpolate between the discrete values of $\mathcal{T}$ as computed for the discrete set of pairs (θ, N).

VII. Results

In this section we test the nonlinear map $\mathcal{T}$ using a nonlinear simulation engine model equipped with variable camshaft timing and coupled with vehicle dynamics. Throughout the simulation we use stoichiometric air-to-fuel ratio $(A/F = 14.64)$, minimum spark advance for best torque $(\sigma = \sigma_{MBT})$, and fourth gear at the modeled automatic transmission. The throttle steps used represent a series of challenging torque demands and test the engine behavior over a wide operating range. The ZEGR engine (ZEGR, solid line in Fig. 16) provides the benchmark torque response for evaluating the dynamically schedulled IEGR engine. Fig. 16 also shows the simulation of the IEGR engine using the developed static camshaft schedule (CT_{static}) and three different transient characteristics: 1) time constant τ_{ct} determined by the non-

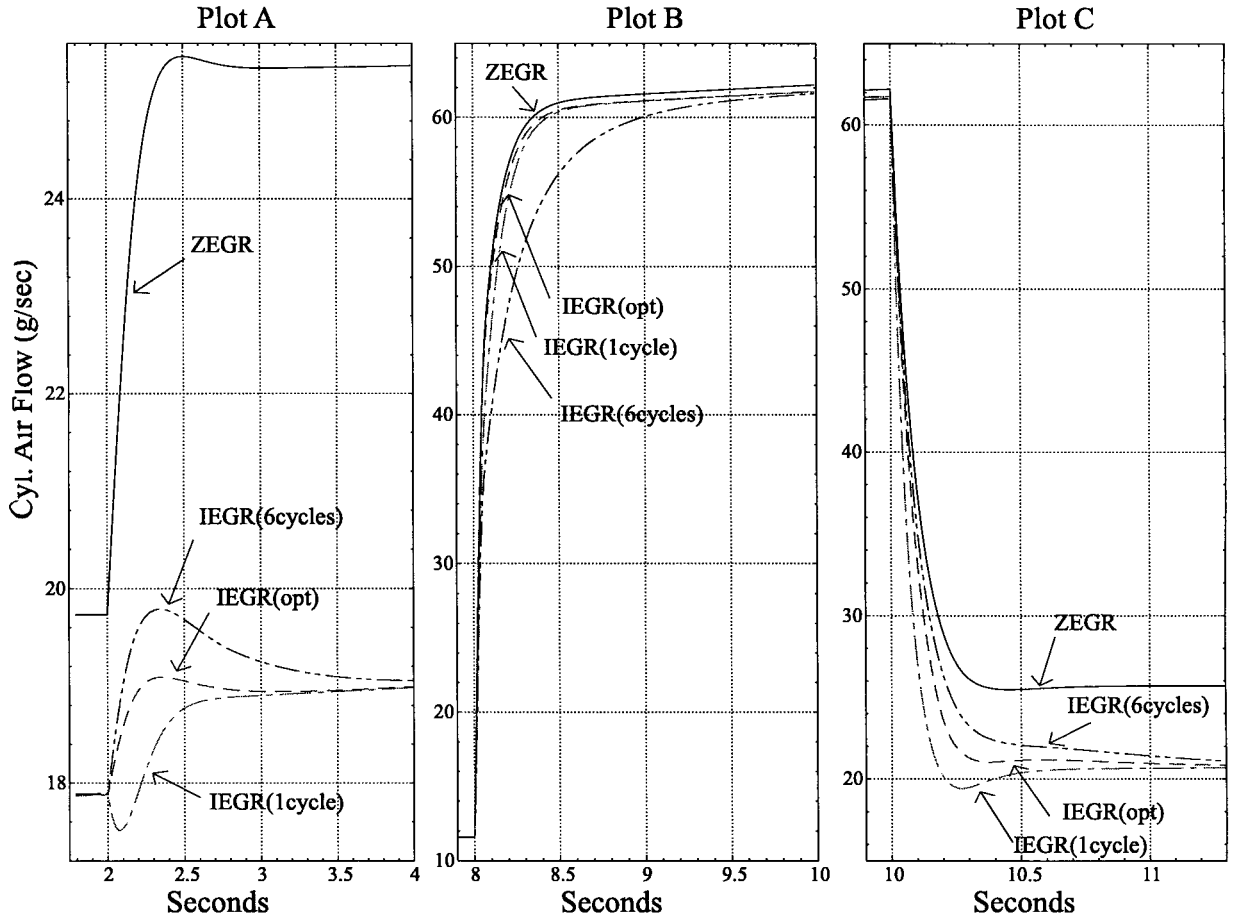

Fig. 17. Dynamic behavior of mass air flow of the four different systems [$ZEGR, IEGR(opt)$, $IEGR$(one cycle), and $IEGR$(six cycles)] during throttle steps.

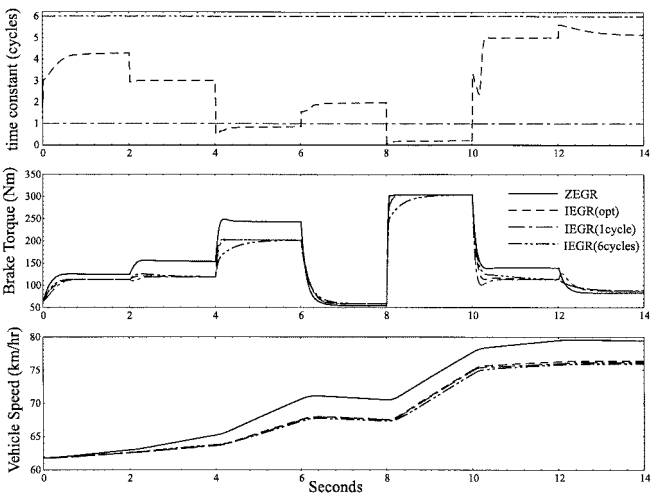

Fig. 18. Nonlinear simulation of the four different systems [$ZEGR, IEGR(opt)$, $IEGR$(one cycle), and $IEGR$(six cycles)] during throttle steps after introducing vehicle dynamics.

linear map $\mathcal{T}$ ($IEGR(opt)$, dashed line); 2) time constant τ_{ct} was chosen to be equal to one engine cycle for all operating condition ($IEGR(1cycle)$, dotted-dashed line); and 3) time constant τ_{ct} was chosen to be equal to six engine cycles for all operating condition ($IEGR(6cycles)$, dotted-dotted-dashed line). Testing the three different IEGR schemes will provide a measure of performance degradation when memory or computing power constraints impose limitations in implementing the fully nonlinear map $\mathcal{T}$.

The differences between the cylinder air flow of ZEGR engine and the IEGR engines are shown in the fifth row of Fig. 16. The subtle differences between the different IEGR dynamic scheduling schemes can be evaluated if we look closer in the A, B, and C areas of the nonlinear simulation.

Fig. 17 magnifies the A, B, and C areas of the nonlinear simulation shown in Fig. 16. At $t = 2$ s (plot A) a small increase in throttle causes the slow IEGR system to exhibit overshoot and the fast IEGR system to exhibit undershoot in the cylinder air flow response. The IEGR engine that uses the time constant as defined by the nonlinear map $\mathcal{T}$ has a smooth response. A slight undershoot, also present in ZEGR engine response, is due to changing engine speed.

At $t = 8$ s (plot B) a large throttle increase causes camshaft timing to return to base camshaft timing (0°). The IEGR engines that manage to do so at a fast rate (both $IEGR(opt)$ and $IEGR(6cycles)$) have similar response to the ZEGR engine, whereas the slow IEGR system varies significantly from the target response.

At $t = 10$ s (plot C) a decrease in throttle angle requires camshaft timing to attain its maximum value (see fourth row

of Fig. 16). During this step change, the fast IEGR system and the slow IEGR system ($IEGR(1cycle)$ and $IEGR(6cycles)$, respectively) overshoot or respond slowly to the change in torque demand. The response achieved by the IEGR engine that uses the nonlinear static map $\mathcal{T}$ matches the ZEGR dynamic response.

Fig. 18 shows the brake torque (second row) and the vehicle velocity (third row) of the ZEGR and the three IEGR engines for the same throttle steps as in Fig. 16. As expected, the simulated brake torque resembles the cylinder air flow response justifying the assumptions made in Section IV.

VIII. Conclusions

Extensive simulations of the developed IEGR dynamic scheduling scheme demonstrate its ability to match the dynamic response of a ZEGR engine. The scheme comprises of a steady-state map used as set points of a tracking problem and a first-order lag that defines the transition between the optimal steady-state points. Both the steady-state set point and the time constant of the first-order lag depend on nonlinear static maps of throttle angle and engine speed, CT_{static} and $\mathcal{T}$, respectively. We investigated two other suboptimal dynamic schedules for the IEGR engine with the goal to demonstrate the subtle but potentially important deterioration of the engine's torque response if $\mathcal{T}$ is not used.

In future work we will concentrate on the implementation and testing of the developed scheme with the variable camshaft timing engine mounted on a transient dynamometer. An adaptive algorithm that modifies the static nonlinear maps $CT_{\text{static}}(\theta(t), N(t))$ and $\mathcal{T}(\theta(t), N(t))$ based on crankangle position measurements will be investigated.

Appendix I
Derivation of τ_{ct}^*

For $\tau_{ct} \geq 1/p_m$

$$K_2(\tau_{ct}) = (0 \mid -c_1 a_{12} - c_2 p_m) + \frac{1}{\tau_{ct}}(0 \mid c_2).$$

Define $\tau_{ct}^* = (c_2/(c_1 a_{12} + c_2 p_m))$, which results, according to (15), in $\tau_{ct}^* = (1/(k_m k_{\theta 2}))$.

Using positiveness of the gains k_m, k_{p2}, we show that $\tau_{ct}^* > (1/p_m)$.

Hence, $K_2(\tau_{ct}^*) = 0$, and $X_0(\tau_{ct}^*, \theta, N) = \boldsymbol{R}^2$.

Appendix II
Time Constant Schedule

The algorithm used is described as follows:

$$\tau_{ct} = \begin{cases} \dfrac{1}{k_m k_{\theta 2}}, & \text{if } k_{\theta 2} \geq k_{\theta 2}^{\min} \\ \dfrac{k_o k_{p1}}{k_{\theta 1} k_m k_{p2}} + \dfrac{1}{2 k_m k_{\theta 2}}, & \text{otherwise} \end{cases} \tag{27}$$

When $k_{\theta 2}$ is small (but nonzero) we can achieve pole zero cancelation but the resulted p_{ct} and z are small when compared to p_m. In this case inexact cancelation of the pole p_{ct} with the zero z might result in unacceptable slow response. Therefore, equilibrium for which $k_{\theta 2} < k_{\theta 2}^{\min}$ should be treated similar to the equilibrium for which $k_{\theta 2} < 0$. In the algorithm used for the simulations shown in Section VII, we chose $k_{\theta 2}^{\min} = 14.5$.

In practice the pole-zero cancelation may not be feasible due to actuator bandwidth constraints. In particular during operation in high intake manifold pressures the bandwidth requirements can be restrictive. In this case we can relax the objective of designing the IEGR engine controller to match the dynamic behavior of the ZEGR engine, and impose the monotonicity constraint in (13). In the region of high manifold pressure (normal flow, $k_{\theta 2} > 0$) the static schedule requires $k_o < 0$, i.e., we start decreasing the dilution to achieve the maximum engine torque (see Section III). The equivalent constraint on τ_{ct} is

$$\tau_{ct} \leq \frac{1 + \lambda_2}{p_m} - \lambda_1 \quad \text{or} \quad \tau_{ct} \geq \frac{\lambda_1}{\lambda_2} \tag{28}$$

where $\lambda_1 = -k_o(k_{\theta 2} k_{p1}/(k_{\theta 1} k_{p2}))$, and $\lambda_2 = -k_o(k_{p1}/(k_m k_{\theta 1} k_{p2}))$. It is easy to verify that $(1 + \lambda_2/p_m) - \lambda_1 < (\lambda_1/\lambda_2)$ and $(\lambda_1/\lambda_2) = (1/(k_m k_{\theta_2})) = \tau_{ct}^*$. By choosing $\tau_{ct} \geq (\lambda_1/\lambda_2)$ we ensure monotonic behavior with dominant pole p_{ct}, $p_m > z \geq p_{ct}$. As a result the throttle-to-torque response of the IEGR engine is slower that the throttle-to-torque response of the ZEGR engine.

Acknowledgment

The authors wish to acknowledge Prof. J. Freudenberg and Prof. E. Gilbert for the helpful discussions and K. Butts for the vehicle simulation model; T. Leone and M. Seaman for the impeccable experimental data; and E. Badillo for the invaluable comments on driveability and engine performance.

References

[1] J. B. Heywood, *Internal Combustion Engine Fundamentals*. New York: McGraw-Hill, 1988.
[2] C. Hsieh, A. G. Stefanopoulou, J. S. Freudenberg, and K. R. Butts, "Emission and drivability tradeoffs in a variable cam timing SI engine with electronic throttle," in *Proc. 1997 Amer. Contr. Conf.*, Albuquerque, NM, 1997, pp. 284–288.
[3] M. Jankovic, F. Frischmuth, A. G. Stefanopoulou, and J. A. Cook, "Torque management of engines with variable cam timing," *IEEE Contr. Syst. Mag.*, vol. 18, pp. 34–42, Oct. 1998.
[4] S. Jayasuriya and J.-W. Song, "On the synthesis of compensators for nonovershooting step response," *ASME J. Dynamic Syst., Measurement, Contr.*, vol. 118, pp. 757–763, 1996.
[5] A. G. Stefanopoulou, J. A. Cook, J. S. Freudenberg, and J. W. Grizzle, "Control-oriented model of a dual equal variable cam timing spark ignition engine," *ASME J. Dynamic Syst., Measurement Contr.*, vol. 120, pp. 257–266, 1998.
[6] A. G. Stefanopoulou and I. Kolmanovsky, "Dynamic scheduling of internal exhaust gas recirculation systems," *Proc. IMECE 1997*, DSC-vol. 61, pp. 671–678.
[7] R. A. Stein, K. M. Galietti, and T. G. Leone, "Dual equal VCT—A variable camshaft timing strategy for improved fuel economy and emissions," SAE Paper 950975.

Anna G. Stefanopoulou (S'93–M'96) received the Diploma degree in 1991 from the National Technical University of Athens, Greece, the M.S. degree in in naval architecture and marine engineering in 1992 and the M.S. and Ph.D. degrees in electrical engineering and computer science in 1994 and 1996, respectively, all from the University of Michigan, Ann Arbor.

She is presently Assistant Professor at the Mechanical Engineering Department at the University of California, Santa Barbara. Her research interests are multivariable feedback theory, control architectures for industrial applications, and powertrain modeling and control.

Dr. Stefanopoulou is Vice-chair of the Transportation Panel in ASME DSCD and a recipient of a 1997 NSF CAREER award.

Ilya Kolmanovsky (S'94–M'95) received the M.S. degrees in Aerospace engineering and mathematics in 1993 and 1995, respectively, and the Ph.D. degree in aerospace engineering in 1995, all from the University of Michigan, Ann Arbor.

He is presently a technical Specialist with Ford Research Laboratory, Dearborn, MI, conducting research on advanced powertrain modeling and control.